Reconstruction of Holocene coupling between the South America Monsoon System and local moisture variability from speleothem $\delta^{18}O$ and $^{87}Sr/^{86}Sr$ records:

Author: Brittany Marie Ward

Reconstruction of Holocene coupling between the South America Monsoon System and local moisture variability from speleothem $\delta^{18}O$ and $^{87}Sr/^{86}Sr$ records

Brittany Marie Ward

A thesis

submitted to the Faculty of

the department of Earth and Environmental Science

in partial fulfillment

of the requirements for the degree of

Master of Science

Boston College
Morrissey College of Arts and Sciences
Graduate School

May 2018

Reconstruction of Holocene coupling between the South America Monsoon System and local moisture variability from speleothem $\delta^{18}O$ and $^{87}Sr/^{86}Sr$ records

Brittany Marie Ward

Advisor: Corinne I. Wong, Ph.D.

Abstract

Investigating controls on past variability of South American hydroclimate is critical to assessing its response to future warming scenarios. $\delta^{18}O$ records from South America offer insight into past variability of the South American Monsoon System (SAMS). The controls on precipitation $\delta^{18}O$ values, however, can be decoupled from precipitation amount and thereby limit investigations of variability in local moisture conditions. Here we use a principle components analysis to assess the coherence of speleothem and lake core Holocene $\delta^{18}O$ records in tropical South America to evaluate the extent to which $\delta^{18}O$ variability reflects changes in SAMS intensity at different sites across the region. The main mode of variability across Holocene $\delta^{18}O$ records (PC1) closely tracks austral summertime insolation, consistent with existing work. PC1 is strongly expressed at sites towards the periphery of the continent, while variability at interior sites bear little similarity that implicates controls, in addition to monsoon intensity, on these $\delta^{18}O$ records. Further, we develop speleothem $^{87}Sr/^{86}Sr$ records spanning the Holocene from Tamboril Cave (Brazilian Highlands), Paraíso Cave (eastern Amazon Basin), Jaraguá Cave (Mato Grosso Plateau), and Botuverá Cave (Atlantic coastal plain) to investigate coupling between reconstructed monsoon variability and local moisture conditions. Speleothem $^{87}Sr/^{86}Sr$ variability is interpreted as a proxy of local moisture conditions, reflecting the degree of water-rock interaction with the cave

host rock as driven by variations in water residence time. Speleothem $^{87}Sr/^{86}Sr$ records from all the sites, except Botuverá cave, do not co-vary with PC1, suggesting that local moisture conditions do not necessary follow variations in monsoon intensity at these interior sites. These speleothem $^{87}Sr/^{86}Sr$ records, however, generally suggest dry mid-Holocene conditions, consistent with interpretations of other paleo-moisture records in the region. These results highlight that dynamics, in addition to SAMS variability, might influence $\delta^{18}O$ variability as well as local moisture conditions at interior sites, and highlight the need for $\delta^{18}O$-independent reconstructions of moisture conditions.

TABLE OF CONTENTS

LIST OF TABLES

LIST OF FIGURES

INTRODUCTION

The South American Monsoon System (SAMS) is a major source of water for municipal, industrial, and agricultural uses, and supports the rich biodiversity of the Amazon Biome. Investigating the response of the SAMS to changes in past climate provides an avenue for understanding how the SAMS might respond to future warming scenarios, and how this will impact water availability across the region. Much attention has been focused on the reconstruction and dynamical understanding of past variability in the intensity of the SAMS, with a critical focus on the oxygen-isotope ($\delta^{18}O$) values preserved in a wide range of archives, including ice cores, tree rings, lake sediments, and speleothems (e.g., Thompson et al., 2000; Ballantyne, 2011; Bird et al., 2011; Cruz et al., 2005). Investigation, however, of the connection in space and time between regional-scale variability in the SAMS and local moisture conditions is limited (Wortham et al., 2017). Investigation of regional and local hydroclimate dynamics during the Holocene, a period characterized by increasing austral summertime insolation, is of particular relevance to understanding the role of climate in the latitudinal dependent timing of Holocene vegetation (e.g., savanna to woodland) shifts (Silva, 2012).

Variations in South American $\delta^{18}O$ records are commonly interpreted to reflect fluctuations in the convective activity within the core monsoon region. Modelling and modern monitoring studies have demonstrated that modern precipitation $\delta^{18}O$ ($\delta^{18}O_{precip}$)

values across much of tropical and subtropical South America are negatively correlated with convective activity and precipitation amount within the core monsoon region (Vuille and Werner, 2005; Vuille et al., 2012). Consequently, $\delta^{18}O$ records from across the region are commonly interpreted to reflect variations in SAMS intensity. Several studies have found striking co-variance in $\delta^{18}O$ variability from records around the region (Vuille et al., 2012; Bird et al., 2011; Kanner et al., 2013), although some work has documented an east-west dipole in $\delta^{18}O$ records suggesting the influence of additional processes relevant to $\delta^{18}O$ variability in northeastern Brazil (e.g., Cruz et al., 2009; Cheng et al., 2013; Lee et al., 2012; Lui and Battisti, 2015). There has been limited recognition, beyond the east-west dipole response in $\delta^{18}O$ values, of differences among records in the region, or discussion of what might be inferred from such differences. A compilation of $\delta^{18}O$ records from across the region demonstrates both similarities and differences in Holocene $\delta^{18}O$ variability (Figure 1; Figure 2). The clear differences among the records lead to the questions, i) where and when is $\delta^{18}O$ variability a proxy of SAMS intensity?, and ii) what additional processes influence $\delta^{18}O$ variability?

It has long been recognized that the strength of $\delta^{18}O_{precip}$ as a proxy of regional monsoon intensity limits the extent to which $\delta^{18}O_{precip}$ reflects local precipitation amount (i.e., moisture conditions) (e.g., Vuille et al., 2012; Wortham et al., 2017). Although it is commonly, and sometimes implicitly, assumed that SAMS intensity drives local moisture conditions, previous work has documented decoupling between them and highlighted the need to use paired, or multiple, independent and distinct hydroclimate proxies to investigate the nature of coupling between regional monsoon intensity and local moisture conditions (Wortham et al., 2017). More specifically, this coupling can be explored using

speleothem $\delta^{18}O$ variability as a proxy for monsoon intensity and speleothem Sr-isotope ($^{87}Sr/^{86}Sr$) variability as a proxy of local moisture conditions (e.g., Banner et al., 1996; Frumkin and Stein, 2004; Oster et al., 2009; Zhou et al., 2009; Vaks et al., 2013; Oster et al., 2014).

Here we leverage existing $\delta^{18}O$ records to assess the coherence of Holocene $\delta^{18}O$ records throughout the region, with sites spanning the northern Andean foothills, eastern Amazon Basin, Mato Grosso Plateau, Brazilian Highlands, and Atlantic coastal plains, to understand where and when $\delta^{18}O$ reflects monsoon intensity, and identify additional processes that drive discordance among sites. We also develop corresponding speleothem $^{87}Sr/^{86}Sr$ records from several of these sites to investigate spatial and temporal variations in the coupling between monsoon variability and local moisture conditions.

1.0 HYDROCLIMATIC SETTING

The hydroclimate of tropical and subtropical South America consists of distinct wet and dry seasons, driven primarily by the SAMS. The onset of the SAMS begins in October and reaches its mature phase in the austral summer (DJF). Seasonal insolation migration leads to differential heating between land and the Atlantic Ocean, resulting in thermal circulation with mid-level atmospheric rising and precipitation occurring over land. During the mature phase, a zone of deep convection is established over the southern Amazon Basin, with core convection centering over ~10-15°S. This intense convection contributes to formation of an upper-level atmospheric high over Bolivia (Bolivian High; 15°S, 65°W) and a low-level atmospheric low over the Chaco region (Chaco Low; ~25°S). This dynamic draws humid air from the core monsoon region southward via the South American low-level jet, which forms as easterly winds across the Amazon Basin are redirected by the Andes (Vera et al., 2006; Berbery and Barros, 2002). The South American low-level jet is present year-round and is strongest during the austral summer, except south of 15°S where the jet is strongest during winter and spring (Berbery and Barros, 2002). Also during the mature phase of the monsoon system, a NW-SE trending convection band, known as the South Atlantic Convergence Zone (SACZ), forms over the Southern Amazon Basin and southern Brazilian Highlands and extends into the western South Atlantic. Demise of the SAMS occurs during austral fall as the core of monsoon convection weakens and migrates northward (Garreaud et al., 2009; Vera et al., 2006). The Intertropical Convergence Zone (ITCZ), while notably distinct and separate from the SAMS, is an important conduit for moisture to the SAMS. The ITCZ follows

the warmest tropical SSTs and is understood to increase SAMS convection in the modern system when displaced more southward (Marengo et al., 2012; Vuille et al., 2012).

The Amazon Basin receives moisture from the tropical Atlantic Ocean year-round via prevailing easterlies (Vera et al., 2006). Annual precipitation is greater than 2,400 mm, with ~30% of total annual precipitation occurring during the mature phase of the monsoon (DJF), and ~70% occurring during the entirety of the wet season (November – June) (Figure 1). The more southerly Mato Grosso Plateau, Brazilian Highlands, and Atlantic Coastal Plain have semi-humid climates, and receive ~1400 mm of annual precipitation. Moisture from these regions is sourced from both the Amazon Basin and the subtropical Atlantic via the SACZ (Vera et al., 2006). Precipitation over the eastern Amazon Basin and Brazilian Highlands is highly seasonal, primarily occurring when the SAMS is active (November-June), whereas the seasonality of precipitation is relatively less severe over the Mato Grosso Plateau and absent over the Atlantic coastal plains (Figure 1). Despite differences in the seasonality of precipitation amount, the seasonality of precipitation $\delta^{18}O$ values is similar across the regions, reflecting i) the isotopic distillation of moisture when the SAMS is active, and ii) the advection of isotopically depleted moisture to regions downstream of the convection core (Vuille et al., 2012).

2.0 $^{87}SR/^{86}SR$ AS A PROXY OF WATER RESIDENCE TIME

Sr-isotope ($^{87}Sr/^{86}Sr$) values in cave dripwater and speleothems can be used as a proxy of local moisture conditions, reflecting the length of water residence time within the vadose zone above the cave. Infiltrating water obtains its initial $^{87}Sr/^{86}Sr$ signature from soil, as the amount of Sr in rainwater is negligible relative to that acquired from the soil. As water infiltrates through the host bedrock, the $^{87}Sr/^{86}Sr$ signature of the water evolves towards that of the bedrock via water-rock interaction (WRI) (i.e., calcite or dolomite recrystallization). The degree of WRI is dictated largely by water residence time within the subsurface above the cave, where increased water residence time enables increased WRI. Drier conditions promote longer water residence time and results in dripwater (or speleothem) $^{87}Sr/^{86}Sr$ values closer to that of the bedrock than the soil, and vice versa under wet conditions. Thus, speleothem $^{87}Sr/^{86}Sr$ variability can potentially reflect relative changes in local wet/dry conditions (Figure 3).

Characterization of $^{87}Sr/^{86}Sr$ compositions of soil, bedrock, cave dripwater, and speleothems at individual cave sites can provide insight on the feasibility of using speleothem $^{87}Sr/^{86}Sr$ values as a proxy of water residence time associated with variability in local moisture conditions. Ideal settings are those in which the $^{87}Sr/^{86}Sr$ signatures of soil and bedrock are distinct. The occurrence of cave dripwater and speleothem $^{87}Sr/^{86}Sr$ values between those of the soil and bedrock is consistent with the conceptual model that the $^{87}Sr/^{86}Sr$ value of infiltrating water is constrained by those of the soil and bedrock. Modelling of the evolution of water geochemical and isotopic compositions due to WRI can provide further means to assess the conceptual model. WRI is a strong control on

cave dripwater and speleothem $^{87}Sr/^{86}Sr$ values, as WRI will increase trace element concentrations relative to calcium (e.g., Sr/Ca) and evolution of $^{87}Sr/^{86}Sr$ values towards that of the bedrock (Banner et al., 1996; Musgrove and Banner, 2004; Wong et al., 2011). The $^{87}Sr/^{86}Sr$ signature of the groundwater evolves towards that of the bedrock as more Sr is progressively acquired from the dissolution of bedrock. The dissolution of bedrock with higher Sr/Ca ratios than the corresponding calcite that is re-precipitated increases Sr/Ca values of the water as bedrock is recrystallized. Calcite precipitation from infiltrating water (i.e., prior calcite precipitation, PCP) results in an increase in Sr/Ca values. Specifically, Ca is preferentially removed from dripwater relative to Sr when calcite precipitates in voids above the cave or on the cave ceiling, thereby increasing the ratio of Sr relative to Ca in the remaining dripwater (Fairchild et al., 2007). Importantly, PCP does not affect $^{87}Sr/^{86}Sr$ compositions, that is, isotopic fraction of Sr is negligible during calcite precipitation remain unchanged. Therefore, calcite precipitation due to the degassing of CO_2 voids above the cave or as water enters the cave will result in the decoupling of the evolution of Sr/Ca and $^{87}Sr/^{86}Sr$ values, making the co-variation of Sr/Ca and $^{87}Sr/^{86}Sr$ values a useful delineator of WRI vs. PCP processes (Wong et al., 2011). Modelling results that can account for observed dripwater compositions indicate that water-rock interaction could be a strong control on cave dripwater and speleothem $^{87}Sr/^{86}Sr$ values at modelled sites.

It is pertinent, however, to note that dripwater $^{87}Sr/^{86}Sr$ values and the magnitude of $^{87}Sr/^{86}Sr$ variability across sampling events can be different between sites within the same cave. Such differences might reflect spatial heterogeneity in soil and/or bedrock $^{87}Sr/^{86}Sr$ values or differences in the dominant type of flow path supplying each site.

With respect to the latter, diffuse flow paths through the matrix pore space of the host rock will reflect longer water residence time, more water-rock interaction, and $^{87}Sr/^{86}Sr$ values that are more similar to those of the bedrock relative to conduit flow paths. Conduit flow paths occur along solution-widened fractures that enable a more direct flow path between the surface and subsurface. Variability in flow rate and isotopic and geochemical compositions of dripwater at sites supplied by conduit flow paths is higher relative to sites supplied by diffuse flow paths that are buffered from changes at the surface. The spatial variability in $^{87}Sr/^{86}Sr$ compositions between sites from the same cave, therefore, requires that caution be taken when considering temporal variability in speleothem $^{87}Sr/^{86}Sr$ values compiled from distinct speleothem samples. That is, offsets in values and differences in the magnitude of variability in $^{87}Sr/^{86}Sr$ values in speleothems from the same cave should be expected and taken into consideration when interpreting changes in moisture conditions over time. Ideally, speleothem $^{87}Sr/^{86}Sr$ would be based on a relative variability within a single speleothem sample. This limitation is less relevant with speleothem $\delta^{18}O$ records, which can more commonly be integrated across distinct speleothem samples with overlapping growth intervals. While differences in the nature of flow paths supplying different sites may still be relevant, spatial and temporal dripwater $\delta^{18}O$ variability is relatively homogenous due to mixing of infiltrating water in the subsurface above the cave (Ayalon et al., 1998; Lachniet, 2009).

3.0 METHODS

This study generated $\delta^{18}O$ and $^{87}Sr/^{86}Sr$ records for a speleothem from Tamboril Cave (TM6), and $^{87}Sr/^{86}Sr$ records for three additional cave sites in Brazil with existing $\delta^{18}O$ records, Paraíso (PAR01, PAR03, and PAR16), Jaraguá (JAR02, JAR04, and JAR07), and Botuverá (BTV21a) Caves. Each cave is hosted by carbonate bedrock within a unique geologic and vegetative setting (Table 1). Each cave site was visited to collect soils, bedrock, and dripwater samples to characterize their $^{87}Sr/^{86}Sr$ compositions. Soils were collected at the cave entrance and at multiple locations above cave when accessible. Bedrock samples were collected at the cave entrance and from several locations within the cave. Dripwater samples were collected from several distinct, actively dripping sites. TM6 is a columnar stalagmite that was found already broken ~500 m into the cave in 2016.

Age constraints (n=12) for TM6 were developed using U series dating methods (Figure 4). Sample preparation and chemical separation of U and Th-fractions were carried out at Boston College Center for Isotope Geochemistry (BC-CIG) and instrumental analyses were carried out the Massachusetts Institute for Technology Paleoclimate and Geochronology Lab (following Edwards et al., 1987) (Supplemental Materials). Powder samples were dissolved and spiked with a ^{233}U-^{229}Th spike based on sample weight, and age and ^{238}U concentration estimates. Spiked samples were prepared for analyses using Fe co-precipitation purification and U and Th ion exchange chromatography following the methods of Edwards et al. (1987). Prepared U and Th samples were analyzed on a Nu Plasma II-ES MC-ICP-MS with a static analysis, with

unknowns bracketed by U and Th standard solutions. ^{234}U and ^{230}Th were measured via ion counter, while remaining masses were measured on Faraday cups. Total procedural blank measurements are < 2.0 pg ^{238}U, <0.8 fg ^{234}U, and undetectable ^{230Th}.

Analyses of $^{87}Sr/^{86}Sr$ values for soil and rock leachates, dripwater, and speleothems were conducted at BC-CIG. Speleothem powder (2 mg) was hand-drilled using a dental drill at discrete 1 cm increments (~200 yr resolution). Dried, disaggregated soils (0.5 g) and crushed bedrock (0.01 g) were leached in 1 M ammonium acetate. All samples were processed using ion exchange methods as detailed by Montañez et al. (2002) and loaded onto outgassed single Re filaments in a TaF loading solution for analyses on an Isotopx Phoenix Thermal Ionization Mass Spectrometer (TIMS) at BC-CIG (ref method). Samples were analyzed using a dynamic analysis. Uncertainty for $^{87}Sr/^{86}Sr$ values measured at BC-CIG is 0.000007 (2σ), based on the standard deviation of SRM987 measurements (mean = 0.710243, n=42). The $^{87}Sr/^{86}Sr$ of a subset of dripwater samples from Tamboril cave was measured at University of Brasilia.

Dripwater, bedrock, and soils from Paraíso, Tamboril, Jaraguá, and Botuverá caves were analyzed for cation concentrations (Ca, Mg, Sr). Dripwater was analyzed using in the Quadrupole ICP-MS Lab in the Department of Geological Sciences at the University of Texas at Austin. Bedrock and soil samples were analyzed as pressed powder pellets using x-ray fluorescence on a Philips PW2400 sequential spectrometer in the Ronald B. Gilmore XRF Lab, University of Massachusetts, Amherst following the methods of Rhodes (1996).

The evolution of dripwater Sr/Ca and $^{87}Sr/^{86}Sr$ values due to WRI was modelled following Banner and Hanson (1990). Here we consider WRI to include calcite or

dolomite recrystallization. Iterative mass balance calculations simulate increments of water passing through a given volume of bedrock (measured in mols), assuming each increment of water comes to elemental and isotopic equilibrium with the bedrock it is in contact with based on the partition coefficients of isotopic and elemental systems. Initial dripwater Sr/Ca values were assigned based on the lowest dripwater Sr/Ca (i.e., least evolved) measured at each cave site. Initial dripwater $^{87}Sr/^{86}Sr$ values were assumed to have the $^{87}Sr/^{86}Sr$ values of soil above each cave (e.g., Banner et al., 1996; Musgrove an Banner, 2004; Wong et al., 2011; Wortham et al., 2017). Two sets of WRI trends are calculated for each cave system using the most and least radiogenic soil and bedrock values measured, which captures the range of possible dripwater values that could evolve under WRI.

Coherence of Holocene $\delta^{18}O$ variability from the region was assessed using a Principle Component Analysis (PCA). Records that spanned 2000 – 9600 yrs BP, and for which raw age-depth and proxy-depth data were accessible, were included. Age-depth models were recalculated for existing records to quantify uncertainty associated with age-depth models and enable equitable comparison across all records (Breitenbach et al., 2012). The COPRA algorithm was used to generate 2000 realizations of each age-model, and therefore, unique $\delta^{18}O$ time series, for each site for all records used in the PCA (Breitenbach et al., 2012). Raw proxy-depth information were not available for $\delta^{18}O$ records for LG3 and LG11 from Lapa Grande (Strikis et al., 2011) and BTV21a from Botuverá records (Bernal et al., 2016). For these samples proxy-depths were estimated using a polynomial regression of the assessable age-depth and proxy-age data, and results were input into COPRA. Unique composite $\delta^{18}O$ records were made for sites for which

there were multiple speleothems by averaging $\delta^{18}O$ values at each time-step in the overlapping interval using the 2,000 unique $\delta^{18}O$ time series for each speleothem sample output from COPRA. The PCA was conducted for each unique set of $\delta^{18}O$ time series.

4.0 RESULTS

Oxygen-isotope records of sites toward the periphery of the continent (i.e., Botuverá, El Condor, Diamente, and Haupago Caves and Laguna Pumacocha) (herein referred to as peripheral sites) exhibit a common decreasing trend that corresponds with increasing austral summer insolation throughout the Holocene (Figure 2) (Cruz et al., 2005a; Cruz et al., 2007; Wang et al., 2008; Kanner et al., 2013; Bird et al., 2011). This decreasing δ18O trend is evident in the first principal component (PC1) delineated from the PCA, on which peripheral sites are all similarly and positively weighted (Figure 5). Sites toward the interior of the continent (Paraíso, Lapa Grande, Tamboril, and Jaraguá caves; here-in referred to as interior sites) do not exhibit a coherent decreasing trend from the early to late Holocene and are not heavily positively weighted on PC1. Additionally, $\delta^{18}O$ records of interior sites exhibit distinct variability that is not consistent across the region as evidenced by disparate weightings on PC1 and PC2.

Soil and bedrock $^{87}Sr/^{86}Sr$ values vary widely between sites. $^{87}Sr/^{86}Sr$ values of soil and bedrock at Tamboril are more radiogenic than those at Paraíso, Jaraguá, and Botuverá, and the difference between soil and bedrock values is greatest at Tamboril. Each site has a similar standard deviation of soil (±0.0008) and bedrock (±0.003) $^{87}Sr/^{86}Sr$ values, except Paraíso, where soil values have a relatively large range (±0.004), but the tightest grouping of bedrock values (±0.0002). Dripwater and speleothem $^{87}Sr/^{86}Sr$ are bracketed by those of soil and bedrock at each site. Tamboril dripwater $^{87}Sr/^{86}Sr$ values are more variable across drip sites than in other caves (±0.0068 vs ±0.001) (Figure 6), although relatively invariant across sampling events.

Soil and bedrock $^{87}Sr/^{86}Sr$ values are distinct at Paraíso, Tamboril, Jaraguá, and Botuverá Cave sites, and modern dripwater and speleothem $^{87}Sr/^{86}Sr$ values are bracketed by soil and bedrock $^{87}Sr/^{86}Sr$ values at each site as well (Figure 6). Observed Sr/Ca and $^{87}Sr/^{86}Sr$ values of dripwater from Paraíso, Tamboril, and Jaraguá caves could largely be accounted for by model WRI curves. Dripwater with higher Sr/Ca values, for a given $^{87}Sr/^{86}Sr$ value, than model WRI curves can be accounted for by prior calcite precipitation (PCP) (Wong et al., 2011).The consistency of the $^{87}Sr/^{86}Sr$ settings across all sites and the coincidence of modelled WRI (and, in some cases, PCP) curves with dripwater at each site support the use of speleothem $^{87}Sr/^{86}Sr$ variability as a proxy of variability in local moisture conditions at each site.

The speleothem $^{87}Sr/^{86}Sr$ records developed in this study do not co-vary i) with each other, ii) with speleothem $\delta^{18}O$ from the respective sites, nor iii) with PC1 delineated from the compilation of $\delta^{18}O$ records from the region, except for Botuverá cave. Botuverá is the only site at which speleothem $^{87}Sr/^{86}Sr$ and $\delta^{18}O$ records exhibit co-variability that is consistent with an interpretation that local moisture conditions became wetter with the increase in regional monsoon intensity over the Holocene (Figure 7). Further, Botuverá speleothem Sr/Ca, $\delta^{234}U$, and growth rate records previously developed by Bernal et al. (2016) are all consistent with this finding, and further support the use of speleothem $^{87}Sr/^{86}Sr$ values as a proxy of moisture conditions. Importantly, however, is the distinct variability in Holocene $\delta^{18}O$ values (BTV21a, Bernal et al., 2016; BTV2, Cruz et al., 2005; BT3, Wang et al., 2007) (Figure 7; Figure S1) over the last 4 ka. This observation highlights the potential for differential preservation of the same climate signal in different samples from the same cave (or from different caves in the same area)

due to the influence of the cave system (e.g., Baker et al., 2010; Wong and Breecker, 2015).

The speleothem $^{87}Sr/^{86}Sr$ record developed from Paraíso contains a negative excursion from 8 to 6 ka, inferred as a dry interval within the $^{87}Sr/^{86}Sr$ proxy framework. This interval is coincident with slower speleothem growth, as evidenced by the age-model, but is not reflected in $\delta^{18}O$. This period coincides with abrupt drying in the Sahara present in paleoclimate and archaeological archives, discussed in detail later (Stager et al., 2003; Tierney et al., 2017). The Paraíso $^{87}Sr/^{86}Sr$ records recovers from the 8 – 6ka excursion to wetter conditions before exhibiting a dry interval in the mid-Holocene (5 to 2 ka). The apparent lack of trend in TM6 relative to TM0 may be a difference of sensitivity of the Sr-proxy between the two speleothems, which were sampled from two different drip sites within a fairly heterogenous cave system (i.e., not a one-to- one relationship between TM0 and TM6 $^{87}Sr/^{86}Sr$ values). Standardization of TM0 and TM6 $^{87}Sr/^{86}Sr$ records individually allows for a more objective analysis of trends within the TM6 record. Standardization of TM6 yields a $^{87}Sr/^{86}Sr$ record that exhibits a step change with high $^{87}Sr/^{86}Sr$ values during the early (10 to 8 ka) relative to the mid and late Holocene (6 to 2ka), which is decoupled from the main monsoon signal (Figure S2). During the last 2 ka at Tamboril cave, however, the $^{87}Sr/^{86}Sr$ record is coupled with increased monsoon intensity as previously discussed (Wortham et al., 2017). Of note, $^{87}Sr/^{86}Sr$ values of the last millenia are antiphased between Tamboril (increasing) and both Paraíso and Botuverá caves (decreasing). The Jaraguá record increases from 10 to 8 ka and decreases from 5 ka to present, marking onset of a mid-Holocene dry interval coincident with Paraíso and Tamboril mid-Holocene (~5 to 2 ka) drying.

Standardization of JAR4 $^{87}Sr/^{86}Sr$ more readily reveals Jaraguá experienced wetting conditions at ~0.5 ka, temporally offset from the onset of wetter conditions at Tamboril, and antiphased with the onset of drying conditions at both Paraíso and Botuverá caves.

5.0 DISCUSSION

5.1 DRIVERS OF REGIONAL ^{18}O DISCORDANCE

Isotope enabled climate modeling and monitoring studies have shown that oxygen isotope variability of precipitation ($\delta^{18}O_{precip}$) in tropical and subtropical South America is driven by the extent of vapor mass distillation, with more depleted values associated with more intense convection over the core monsoon region (e.g., Vuille et al., 2003; Hardy et al., 2003; Vuille and Werner, 2005; Vuille et al., 2012). This framework defines the paradigm for reconstructing SAMS activity from $\delta^{18}O$ variability preserved in a wide range of archives, including ice cores (Thompson et al., 2010; Thompson et al., 1995), lake sediments (Bird et al., 2011), tree rings (Ballantyne et al., 2011) and speleothems (e.g., Burns et al., 2015; Strikis et al., 2018), from the area. Modeling studies investigating the response of precipitation amount and precipitation $\delta^{18}O$ values to past climate forcings have provided additional insight into potential climate dynamics represented by $\delta^{18}O$ records from across the region (e.g., Lee et al., 2009; Lewis et al., 2010). For example, orbitally paced changes in insolation result in a dipole response in precipitation $\delta^{18}O$ between the northern Andes and Nordeste region, with i) changes in the northern Andes resulting from differences in the proportion of summer vs. winter precipitation associated with strengthen and weakening of the SAMS and ii) changes in

the Nordeste resulting from the intensification and latitudinal shifts in the ITCZ driven by teleconnections with Africa (Liu and Battisti, 2015).

With respect to variability in Holocene $\delta^{18}O$ records, our analysis has demonstrated that records from peripheral sites (i.e., northern Andes and Atlantic coastal plain) exhibit a gradual shift from higher to lower $\delta^{18}O$ values from early to late-Holocene. This trend is consistent with i) increasing austral summer insolation driving an enhanced land-sea temperature gradient and more intense convection (Bird et al., 2011; Kanner et al., 2012), and ii) changes in trace element concentrations in the sediments of the Cariaco Basin interpreted to reflect a southward shift of the ITCZ (Haug et al., 2001), which is a major moisture flux conduit that fuels convective activity in the SAMS region (Vuille et al., 2012). The lack of this trend, however, in $\delta^{18}O$ records at the other sites demonstrates that the inferred Holocene increase in monsoon intensity is not preserved in all records from the monsoon region. This indicates that precipitation $\delta^{18}O$ values at these sites are not sensitive to Holocene variations in insolation or strength and position of the ITCZ, or that other processes affecting precipitation $\delta^{18}O$ are also influential at these sites.

Dipole $\delta^{18}O$ variability between records from the northern Andes and eastern Amazon Basin and Nordeste has long been recognized (Cruz et al., 2009; Cheng et al., 2013; Lui and Battisti, 2015), although is not consistently present throughout the entirely of the Holocene. The dipole is associated with the linked Bolivian High-Nordeste Low system (Lenters and Cook, 1997), and is apparent in the mid to late-Holocene (6 to 3 ka). That is, $\delta^{18}O$ values increase in records from Paraíso and Rio Grande do Norte, and decrease in records from the northern Andes. During the early Holocene (8 to 10 ka),

however, that dipole is absent as all records from the region exhibit decreasing $\delta^{18}O$ values. The dynamic extent to which the Bolivian High-Nordeste Low system influences $\delta^{18}O$ values in the Nordeste region, which has also been documented over the last millennium (Novello et al., 2013), suggests an additional control on $\delta^{18}O$ variability during the early Holocene. Notably, the $\delta^{18}O$ records at Paraíso and Rio Grande do Norte correspond with Holocene changes in trace element concentrations in the sediments of the Cariaco Basin over this interval, as well as throughout much of the entirety of the Holocene (Figure 9). There is, however, seeming discordance in the dynamical interpretation, as i) changes in the geochemistry of sediments of the Cariaco Basin reflect latitudinal shifts in the ITCZ with greater Ti concentrations corresponding with more *northerly* position of the ITCZ, and ii) precipitation $\delta^{18}O$ values over northeast Brazil correspond to the strength and position of the ITCZ, with lower $\delta^{18}O$ values associated with a more intense and *southerly* position of the ITCZ. The coincidence of higher Ti concentrations in Cariaco Basin sediments and lower $\delta^{18}O$ values in speleothem records from Paraíso and Rio Grande do Norte caves, highlights that the shifts in the ITCZ cannot account for Holocene variations present in both regions.

The records from Jaraguá, Tamboril, and Lapa Grande are similar in their lack of trend in Holocene $\delta^{18}O$ values and discordance with other Holocene $\delta^{18}O$ records from the region. The lack of trend indicates that $\delta^{18}O$ variability at these sites is not sensitive to Holocene variability in the SAMS associated with austral insolation or position of the ITCZ. These sites are proximal to the South Atlantic Convergence Zone (SACZ), which might indicate that climate dynamics driving the strength and position of the SACZ might be an important influence on the $\delta^{18}O$ variability in these records. Grutas de Botuverá,

however, is also located within the SACZ, complicating this hypothesis as its $\delta^{18}O$ record co-varies with those from the northern Andes, indicating sensitivity to SAMS variability, and not with those from sites that also located within proximity of the SACZ.

5.2 (DE)COUPLING OF LOCAL MOISTURE CONDITIONS AND REGIONAL MONSOON INTENSITY

Of the four $^{87}Sr/^{86}Sr$ records developed in this study, only Botuverá cave illustrates coupling with regional monsoon variability over the Holocene, suggesting moisture availability in Atlantic coastal plain region might have been linked with increasing monsoon intensity (Figure 7; Figure 8). Lack of consistency between speleothem $^{87}Sr/^{86}Sr$ records and regional monsoon intensity at the other sites suggests that regional monsoon variability may not be a dominant control on local moisture conditions across the region. The coincidence, however, of variability in $^{87}Sr/^{86}Sr$ records with other records from the region may provide insight into climate processes that may be pertinent to Holocene variations in local moisture at each site.

The coincidence of the negative excursion in the Paraíso $^{87}Sr/^{86}Sr$ record and the onset and demise of a drying event in northern Africa from 8 to 6 ka suggests a dynamic link between the two regions. A pause from 8 to 6 ka in the otherwise humid early to mid-Holocene Green Saharan period is inferred from leaf wax δD records from off-shore ocean and lake sediments and lake level and archeological records (Tierney et al. 2017).

Tierney et al. (2017) suggest the North African drying from 6 to 8 ka may reflect a prolonged response to the 8.2 ka event due to vegetation feedbacks that altered albedo and weakened the monsoon. The 8.2 ka event marks a meltwater pulse to the North Atlantic and slow down of the Atlantic Meridional Overturning Circulation, lasting for a couple hundred years with disruptions in Northern Hemisphere climate patterns typically lasting several hundred years (Alley et al., 1997). Modelling studies have demonstrated that both changes in Atlantic sea surface temperatures (SSTs) and land heating over Africa can drive teleconnections that influence precipitation patterns over northeastern Brazil (Lui and Battisti, 2015, Cook et al., 2004). Simulations of the 8.2ka event demonstrate negative precipitation anomalies over both northern Africa and the northern Amazon Basin, including the region in which Paraíso cave is located and positive precipitation anomalies over the Brazilian Nordeste region (Matero et al., 2017). As in Africa, the perturbation in moisture conditions inferred from the Paraíso Sr-isotope record persist beyond the relatively rapid 8.2 ka event, necessitating a mechanism for prolonging the precipitation anomaly in the region. While delineation of such a mechanism is beyond the scope and capability of this study, we posit that teleconnections resulting from the sustained anomaly in atmospheric conditions over Africa may be a potential explanation.

Decreases in $^{87}Sr/^{86}Sr$ records from Paraíso (6 ka), Tamboril (between 6 and 7ka), and Jaraguá (5ka) within individual speleothems suggests the occurrence of drier, relative to the early Holocene, mid Holocene conditions (Fig. 7 and Sup Fig. 2-3). The onset, though poorly constrained, is broadly coincidental with a period of mid-Holocene drying documented in Andean lake records (~7-3 ka) (e.g., Lake Titicaca, Paco Cocha)

(e.g., Cross et al., 2001; Baker et al., 2001; Abbott et al., 2003, Tapia et al., 2003; Fritz et al., 2007; Pollisar et al., 2013) and retreat of Andean glaciers (8-4 ka) (e.g., Cordillera Blanca (9oS) and Huagurucho (10oS)) inferred from cosmogenic radionuclide ages and proglacial lake sediment flux records (Stansell et al., 2017; Stansell et al., 2014). Records of leaf wax δD and $\delta^{13}C$ from Laguna la Gaiba (18°S, 58°W) located between Tamboril and Jaraguá Caves also indicate drier conditions from 8 to 5 ka (Fornace et al., 2016). This general mid Holocene drying is followed by a transition to wetter conditions in the late-Holocene (~2 ka) at all the sites discussed. The occurrence of a drier mid-Holocene interval is further supported by archeological studies in the tropical Andes and La Plata Basin regions that suggest movements of people out of increasingly more arid environments at this time (e.g., Iriate et al., 2017; Marcelo et al., 2018). Teleconnections resulting from the patterns of tropical Pacific SSTs have been proposed as the control on Holocene variability in the region's hydroclimate based on the pattern of spatial variability in mid Holocene wetting and drying across Latin America (20°N to 20°S) being similar to that resulting from modern day ENSO variations (Pollisar et al., 2013). The occurrence, however, of mid Holocene drying that spans the eastern Amazon Basin, Mato Grosso Plateau, Brazilian Highlands, and Andes is not consistent with the modern response of hydroclimate to ENSO variations. That is, ENSO variability induces a dipole response between the regions of eastern Amazon Basin/Andes and Mato Grosso Plateau and Brazilian Highlands (Garreaud et al., 2009).

There is correspondence between the $^{87}Sr/^{86}Sr$ record from Jaraguá, $\delta^{18}O$ records from Paraíso and Rio Grande do Norte Caves, and the geochemical record from the Cariaco Basin %Ti, which does not entirely align with the trend of PC1 or austral

summer insolation (Figure 9). The coherence of these records could be coincidence or implicate a dynamic promoting dipole moisture conditions between the Mato Grosso Plateau and watershed of the Orinoco River that drains to the Cariaco Basin that is an important control on $\delta^{18}O$ values in precipitation falling over the Nordeste region and eastern Amazon Basin. Additionally, such a dynamic would have limited influence on Holocene variability in monsoon intensity or moisture conditions throughout much of the rest of the region. A mechanism is not readily obvious; however, we again suggest that the ITCZ cannot properly account for these observed trends because of the previously discussed enigma between Cariaco Basin %Ti and Paraíso and Rio Grande do Norte $\delta^{18}O$ records.

$^{87}Sr/^{86}Sr$ records from Paraíso and Tamboril caves suggest antiphased moisture availability over the last millennia between the eastern Amazon Basin (drying) and Brazilian Highlands (wetting). Previous work highlighted a consistent decreasing $\delta^{18}O$ trend over the last millennium in records from the Andean foothills and Mato Grosso Plateau inferred to reflect increasing monsoon intensity, which is consistent with wetter conditions at Tamboril (Wortham et al., 2017). A trend toward drier conditions at Paraíso is consistent with increasing $\delta^{18}O$ from both Paraíso Cave and Diva Cave (eastern Brazil) that suggest a decrease in convection locally, or upstream of the sites, and/or diminished contribution of monsoon-season precipitation. This east-west moisture dipole inferred from the $^{87}Sr/^{86}Sr$ records, however, is dynamic during the Holocene, as dry mid Holocene conditions may have spanned both regions.

Temporal variability in the degree of coherency between $^{87}Sr/^{86}Sr$ records from the Eastern Amazon Basin, Brazilian Highlands, and Mato Grosso Plateau regions

suggests the presence of multiple mechanisms that modulate variability in Holocene moisture conditions, and further, that these mechanisms are regionally heterogeneous. The presence of co-variability among moisture reconstructions from across the region at times during the Holocene indicates that some of these mechanisms have the potential to drive hydroclimate patterns across the region. On the other hand, the lack of co-variability at times suggests a greater influence of local dynamics.

6.0 SUMMARY AND CONCLUSIONS

The work presented here focuses on analyzing the coherence of existing Holocene speleothem and lake core $\delta^{18}O$ records and the relationship between $\delta^{18}O$ records and local moisture reconstructions. A new Holocene $\delta^{18}O$ record is developed for the Brazilian Highlands region, and speleothem $^{87}Sr/^{86}Sr$ records are developed for the eastern Amazon Basin, Brazilian Highlands, Mato Grosso Plateau, and Atlantic Coastal Plain regions. Our results suggest the main mode of variability in Holocene tropical South America $\delta^{18}O$ records is one that closely tracks increasing austral summertime insolation, consistent with existing literature that suggests insolation drives monsoon convection via modulation of the land-sea heat gradient. However, only $\delta^{18}O$ records from the tropical Andean foothills and Atlantic Coastal Plain are positively correlated with this mode, suggesting the other $\delta^{18}O$ records from more interior sites in the eastern Amazon Basin, Brazilian Highlands, and Mato Grosso Plateau are driven by mechanisms beyond monsoon intensity. Such mechanisms are not clear and call for future research. We demonstrate that speleothem $^{87}Sr/^{86}Sr$ values are a feasible proxy of local moisture conditions. Holocene $^{87}Sr/^{86}Sr$ records exhibit variability that is decoupled with the main monsoon signal, suggesting that local moisture conditions are *not* tightly linked to regional monsoon variability. Botuverá cave, however, does exhibit a $^{87}Sr/^{86}Sr$ record that follows monsoon variability throughout the Holocene, suggesting moisture availability in the Atlantic Coastal Plain region may be linked to monsoon intensity. The $^{87}Sr/^{86}Sr$ records are broadly discordant with each other over much of the Holocene, although most of the records exhibit concordant shifts, such as the mid-Holocene drying at ~6 ka in the

eastern Amazon Basin, Brazilian Highlands, and Mato Grosso Plateau, which are consistent with existing lake records from the Andes and Mato Grosso Plateau. This widespread mid-Holocene dry interval, despite monotonic increases in regional monsoon intensity over this interval suggests a mechanism, in addition to monsoon intensity, that modulates precipitation patterns. It is clear that Holocene variability in hydroclimate over tropical and subtropical South America is complex with multiple mechanisms at play. This realization marks the importance of delineating potential controls on speleothem-based proxy records and taking a multi-proxy approach to exploring hydroclimate conditions across the SAMS region.

References

Abbott, M.B., Seltzer, G.O., Kelts, K.R., and Southon, J., 1997, Holocene paleohydrology of the tropical Andes from lake records: Quaternary Research, v. 47, no. 1, p. 70-80.

Abbott, M.B., Wolfe, B.B., Wolfe, A.P., et al., 2003, Holocene paleohydrology and glacial history of the central Andes using multiproxy lake sediment studies: Palaeogeography, Palaeoclimatology, Palaeoecology, v. 194, no. 1-3, p. 123-138.

Alley, R. B., Mayewski, P. A., Sowers, T., Stuiver, M., Taylor, K. C., & Clark, P. U., 1997, Holocene climatic instability: A prominent, widespread event 8200 yr ago. Geology, v. 25, no. 6, p. 483-486.

Baker, P.A., Seltzer, G.O., Fritz, S.C., et al., 2001a, The history of South American tropical precipitation for the past 25,000 years: Science, v. 291, no. 5504, p. 640-643.

Ballantyne, A.P., Baker, P.A., Chambers, J.Q., Villalba, R., and Argollo, J., 2011, Regional differences in South American monsoon precipitation inferred from the growth and isotopic composition of tropical trees: Earth Interactions, v. 15, no. 5, p. 1-35.

Banner, J.L., and Hanson, G.N., 1990, Calculation of simultaneous isotopic and trace element variations during water-rock interaction with applications to carbonate diagenesis: Geochimica et Cosmochimica Acta, v. 54, no. 11, p. 3123-3137.

Banner, J.L., Musgrove, M., Asmerom, Y., Edwards, R.L., and Hoff, J.A., 1996, High-resolution temporal record of Holocene ground-water chemistry: Tracing links between climate and hydrology: Geology, v. 24, no. 11, p. 1049-1053.

Berbery, E.H., and Barros, V.R., 2002, The hydrologic cycle of the La Plata basin in South America: Journal of Hydrometeorology, v. 3, no. 6, p. 630-645.

Bernal, J.P., Cruz, F.W., Strikis, N.M., et al., 2016, High-resolution Holocene South American monsoon history recorded by a speleothem from Botuverá Cave, Brazil: Earth and Planetary Science Letters, v. 450, p. 186-196.

Bird, B.W., Abbott, M.B., Vuille, M., Rodbell, D.T., Stansell, N.D., and Rosenmeier, M.F., 2011, A 2,300-year-long annually resolved record of the South American summer monsoon from the Peruvian Andes: Proceedings of the National Academy of Sciences, v. 108, no. 21, p. 8583-8588.

Breitenbach, S.F., Rehfeld, K., Goswami, B., et al., 2012, Constructing proxy records from age models (COPRA): Climate of the Past, v. 8, no. 5, p. 1765-1779.

Cheng, H., Sinha, A., Cruz, F.W., et al., 2013, Climate change patterns in Amazonia and biodiversity: Nature communications, v. 4, p. 1411.

Cook, K.H., Hsieh, J.S., and Hagos, S.M., 2004, The Africa–South America intercontinental teleconnection: Journal of Climate, v. 17, no. 14, p. 2851-2865.

Cross, S.L., Baker, P.A., Seltzer, G.O., Fritz, S.C., and Dunbar, R.B., 2001, Late Quaternary climate and hydrology of tropical South America inferred from an isotopic and chemical model of Lake Titicaca, Bolivia and Peru: Quaternary Research, v. 56, no. 1, p. 1-9.

Cruz Jr, F.W., Burns, S.J., Jercinovic, M., Karmann, I., Sharp, W.D., and Vuille, M., 2007, Evidence of rainfall variations in Southern Brazil from trace element ratios (Mg/Ca and Sr/Ca) in a Late Pleistocene stalagmite: Geochimica et Cosmochimica Acta, v. 71, no. 9, p. 2250-2263.

Cruz Jr, F.W., Burns, S.J., Karmann, I., et al., 2005a, Insolation-driven changes in atmospheric circulation over the past 116,000 years in subtropical Brazil: Nature, v. 434, no. 7029, p. 63.

Cruz, F.W., Vuille, M., Burns, S.J., et al., 2009, Orbitally driven east–west antiphasing of South American precipitation: Nature Geoscience, v. 2, no. 3, p. 210.

Curtis, J.H., Brenner, M., and Hodell, D.A., 1999, Climate change in the Lake Valencia Basin, Venezuela,~ 12600 yr BP to present: The Holocene, v. 9, no. 5, p. 609-619.

Edwards, R.L., Chen, J.H., and Wasserburg, G.J., 1987, 238U234U230Th232Th systematics and the precise measurement of time over the past 500,000 years: Earth and Planetary Science Letters, v. 81, no. 2-3, p. 175-192.

Fornace, K.L., Whitney, B.S., Galy, V., Hughen, K.A., and Mayle, F.E., 2016, Late Quaternary environmental change in the interior South American tropics: new insight from leaf wax stable isotopes: Earth and Planetary Science Letters, v. 438, p. 75-85.

Fritz, S.C., Baker, P.A., Seltzer, G.O., Ballantyne, A., Tapia, P., Cheng, H., and Edwards, R.L., 2007, Quaternary glaciation and hydrologic variation in the South American tropics as reconstructed from the Lake Titicaca drilling project: Quaternary Research, v. 68, no. 3, p. 410-420.

Garreaud, R.D., Vuille, M., Compagnucci, R., and Marengo, J., 2009, Present-day south american climate: Palaeogeography, Palaeoclimatology, Palaeoecology, v. 281, no. 3-4, p. 180-195.

Haug, G.H., Hughen, K.A., Sigman, D.M., Peterson, L.C., and R&#xFFFD;hl, U., 2001, Southward migration of the intertropical convergence zone through the Holocene: Science, v. 293, no. 5533, p. 1304-1308.

Kanner, L.C., Burns, S.J., Cheng, H., Edwards, R.L., and Vuille, M., 2013, High-resolution variability of the South American summer monsoon over the last seven millennia: insights from a speleothem record from the central Peruvian Andes: Quaternary Science Reviews, v. 75, p. 1-10.

Lachniet, M.S., 2009, Climatic and environmental controls on speleothem oxygen-isotope values: Quaternary Science Reviews, v. 28, no. 5-6, p. 412-432.

Lee, J., Johnson, K., and Fung, I., 2009, Precipitation over South America during the Last Glacial Maximum: an analysis of the “amount effect” with a water isotope-enabled general circulation model: Geophysical Research Letters, v. 36, no. 19.

Liu, X., and Battisti, D.S., 2015, The influence of orbital forcing of tropical insolation on the climate and isotopic composition of precipitation in South America: Journal of Climate, v. 28, no. 12, p. 4841-4862.

Lenters, J. D., & Cook, K. H., 1997, On the origin of the Bolivian high and related circulation features of the South American climate. Journal of the Atmospheric Sciences, v. 54, no. 5, p. 656-678.

Matero, I., Gregoire, L.J., Ivanovic, R.F., Tindall, J.C., and Haywood, A.M., 2017a, The 8.2 ka cooling event caused by Laurentide ice saddle collapse: Earth and Planetary Science Letters, v. 473, p. 205-214.

Mayle, F.E., and Power, M.J., 2008, Impact of a drier Early–Mid-Holocene climate upon Amazonian forests: Philosophical Transactions of the Royal Society B: Biological Sciences, v. 363, no. 1498, p. 1829-1838.

Musgrove, M., and Banner, J.L., 2004, Controls on the spatial and temporal variability of vadose dripwater geochemistry: Edwards aquifer, central Texas1: Geochimica et Cosmochimica Acta, v. 68, no. 5, p. 1007-1020.

Rodbell, D.T., Seltzer, G.O., Mark, B.G., Smith, J.A., and Abbott, M.B., 2008, Clastic sediment flux to tropical Andean lakes: records of glaciation and soil erosion: Quaternary Science Reviews, v. 27, no. 15-16, p. 1612-1626.

Stager, J.C., Cumming, B.F., and Meeker, L.D., 2003, A 10,000-year high-resolution diatom record from Pilkington Bay, Lake Victoria, East Africa: Quaternary Research, v. 59, no. 2, p. 172-181.

Stansell, N.D., Licciardi, J.M., Rodbell, D.T., and Mark, B.G., 2017, Tropical ocean-atmospheric forcing of Late Glacial and Holocene glacier fluctuations in the Cordillera Blanca, Peru: Geophysical Research Letters, v. 44, no. 9, p. 4176-4185.

Stansell, N.D., Polissar, P.J., Abbott, M.B., Bezada, M., Steinman, B.A., and Braun, C., 2014, Proglacial lake sediment records reveal Holocene climate changes in the Venezuelan Andes: Quaternary Science Reviews, v. 89, p. 44-55.

Strikis, N.M., Cruz, F.W., Cheng, H., et al., 2011, Abrupt variations in South American monsoon rainfall during the Holocene based on a speleothem record from central-eastern Brazil: Geology, v. 39, no. 11, p. 1075-1078.

Tapia, P.M., Fritz, S.C., Baker, P.A., Seltzer, G.O., and Dunbar, R.B., 2003, A Late Quaternary diatom record of tropical climatic history from Lake Titicaca (Peru and Bolivia): Palaeogeography, Palaeoclimatology, Palaeoecology, v. 194, no. 1-3, p. 139-164.

Thompson, L.G., Mosley-Thompson, E., and Henderson, K.A., 2000, Ice-core palaeoclimate records in tropical South America since the Last Glacial Maximum: Journal of Quaternary Science, v. 15, no. 4, p. 377-394.

Thompson, L.G., Mosley-Thompson, E., Davis, M.E., et al., 1995, Late glacial stage and Holocene tropical ice core records from Huascaran, Peru: Science, v. 269, no. 5220, p. 46-50.

Tierney, J.E., and Pausata, F.S., 2017, Rainfall regimes of the Green Sahara: Science advances, v. 3, no. 1, p. e1601503.

Vera, C., Silvestri, G., Liebmann, B., and González, P., 2006, Climate change scenarios for seasonal precipitation in South America from IPCC-AR4 models: Geophysical Research Letters, v. 33, no. 13.

Vuille, M., Bradley, R.S., Werner, M., Healy, R., and Keimig, F., 2003, Modeling $\delta^{18}O$ in precipitation over the tropical Americas: 1. Interannual variability and climatic controls: Journal of Geophysical Research: Atmospheres, v. 108, no. D6.

Vuille, M., Burns, S.J., Taylor, B.L., et al., 2012, A review of the South American monsoon history as recorded in stable isotopic proxies over the past two millennia: Climate of the Past, v. 8, no. 4, p. 1309-1321.

Vuille, M., and Werner, M., 2005, Stable isotopes in precipitation recording South American summer monsoon and ENSO variability: observations and model results: Climate Dynamics, v. 25, no. 4, p. 401-413.

Wang, X., Auler, A.S., Edwards, R.L., et al., 2007, Millennial-scale precipitation changes in southern Brazil over the past 90,000 years: Geophysical Research Letters, v. 34, no. 23.

Wang, X., Edwards, R.L., Cruz Jr, F.W., Cheng, H., and Auler, A.S., 2008, Millennial-scale climate variability recorded in Brazilian speleothems.

Wong, C.I., Banner, J.L., and Musgrove, M., 2011, Seasonal dripwater Mg/Ca and Sr/Ca variations driven by cave ventilation: Implications for and modeling of speleothem paleoclimate records: Geochimica et Cosmochimica Acta, v. 75, no. 12, p. 3514-3529.

Wong, C.I., and Breecker, D.O., 2015, Advancements in the use of speleothems as climate archives: Quaternary Science Reviews, v. 127, p. 1-18.

Wortham, B.E., Wong, C.I., Silva, L.C., et al., 2017, Assessing response of local moisture conditions in central Brazil to variability in regional monsoon intensity using speleothem 87 Sr/86 Sr values: Earth and Planetary Science Letters, v. 463, p. 310-322.

Tables

Table 1: Site Descriptions

Cave	Location	Host Geology	Primary Lithology	Bedrock Overburden (m)	Soil Thickness (cm)	Vegetative Cover	References
Paraíso	4°S, 55°W (60 m asl)	Itaituba Fm / Tapajós Group (Paleozoic)	Limestone	15	> 100	Thick tropical forest cover year round	Wang et al., 2017; this study
Jaraguá	21°S, 56°W (570 m asl)	Bocaina Fm / Corumbá Group (Neoproterozoic)	Dolomite	~5	20	Semi-deciduous cover and Cerrado surrounding	Novello et al., 2017
Tamboril	16°S, 47°W (600 m asl)	Sete Lagos Fm / Bambui Group (Neoproterozoic)	Dolomite (w/ interbedded marls and siltstone)	~10 - 50	~10 - 20	Semi-deciduous cover and Cerrado surrounding	Silva et al., 2001; Wortham et al., 2017; this study
Botuverá	27°S, 49°W (230 m asl)	Botuvera Fm / Brusque Group (Neoproterozoic)	Dolomite and carbonate sediments within metavolcanoclastic sequence	~ 70	>100	Thick tropical Atlantic rainforest	Cruz et al., 2007; Bernal et al., 2016

Table 2: U/Th data for TM6

Figures

Sample ID	Depth (mm)	^{238}U (ng/g)[a]	± (2σ)	^{232}Th (pg/g)[a]	± (2σ)	$\delta^{234}U$ (per mil)[b]	± (2σ)	($^{230}Th/^{238}U$) activity	± (2σ)	$^{230}Th/^{232}Th$ ppm atomic	± (2σ)	Age (yr) (uncorr)[c]	± (2σ)	Age (yr) (corr)[d]	± (2σ)	$\delta^{234}U$ initial (per mil)[e]	± (2σ)	Age (yr B.P)
TM6-T	2	8380	170	944	19	832.4	0.6	0.01718	0.00008	2420	11	1026	5	1025	5	834.8	0.6	958
TM6-16	16	6840	140	2230	50	840.5	0.7	0.02069	0.00014	1006	12	1232	8	1226	9	843.4	0.7	1159
TM6-36	36	5070	100	300	20	874.8	1.2	0.02385	0.00017	6400	400	1395	10	1394	10	878.3	1.2	1327
TM6-55	55	6560	130	186	19	852	0.6	0.0253	0.00015	14200	1400	1498	9	1498	9	855.6	0.6	1431
TM6-80	80	6950	140	710	30	815.3	1.6	0.02767	0.00013	4290	130	1673	8	1672	8	819.1	1.6	1605
TM6-93	93	3660	70	2770	60	849.9	0.8	0.0587	0.0002	1233	9	3509	15	3496	16	858.4	0.8	3429
TM6-115	115	3900	80	1270	30	870.7	0.8	0.0641	0.0002	3130	40	3794	13	3788	14	880	0.8	3721
TM6-117	117	17300	300	870	30	742.7	0.8	0.0887	0.0002	28000	600	5676	15	5675	15	754.7	0.8	5608
TM6-138	138	7050	140	3820	80	727.3	1.7	0.0904	0.0003	2646	13	5839	19	5830	20	739.3	1.8	5763
TM6-153	153	3040	60	160	20	582.5	0.7	0.1043	0.0004	32000	4000	7400	30	7400	30	594.7	0.7	7333
TM6-173	173	2570	50	210	20	601.6	1	0.1131	0.0004	22000	2000	7950	30	7950	30	615.3	1	7883
TM6-B	209	4080	80	370	7	607.3	1	0.1346	0.0004	23530	70	9490	30	9490	30	623.8	1	9423
TM6-191	191	2570	50	18300	400	607.9	0.8	0.1127	0.0004	252.2	0.9	7890	30	7760	70	621.3	0.8	7693

Notes:

[a]Reported errors for ^{238}U and ^{232}Th concentrations are estimated to be ±1% due to uncertainties in spike concentration; analytical uncertainties are smaller.

[b]$\delta^{234}U = ([^{234}U/^{238}U]_{activity} - 1) \times 1000$.

[c]$[^{230}Th/^{238}U]_{activity} = 1 - e^{-\lambda_{230}T} + (\delta^{234}U_{measured}/1000)[\lambda_{230}/(\lambda_{230} - \lambda_{234})](1 - e^{-(\lambda_{230} - \lambda_{234})T})$, where T is the age. "Uncorrected" indicates that no correction has been made for initial ^{230}Th.

[d]Ages are corrected for detrital ^{230}Th assuming an initial $^{230}Th/^{232}Th$ of (XX±XX) x 10^{-6}.

[e]$\delta^{234}U_{initial}$ corrected was calculated based on ^{230}Th age (T), i.e., $\delta^{234}U_{initial} = \delta^{234}U_{measured} X e^{\lambda_{234} * T}$, and T is corrected age.

[f]B.P. stands for "Before Present" where the "Present" is defined as the January 1, 1950 C.E.

Decay constants for ^{230}Th and ^{234}U are from Cheng et al. (2013); decay constant for ^{238}U is 1.55125 x 10^{-10} yr^{-1} (Jaffey et al., 1971).

TM6-191 was not included in the age model due to due non-monotonic nature

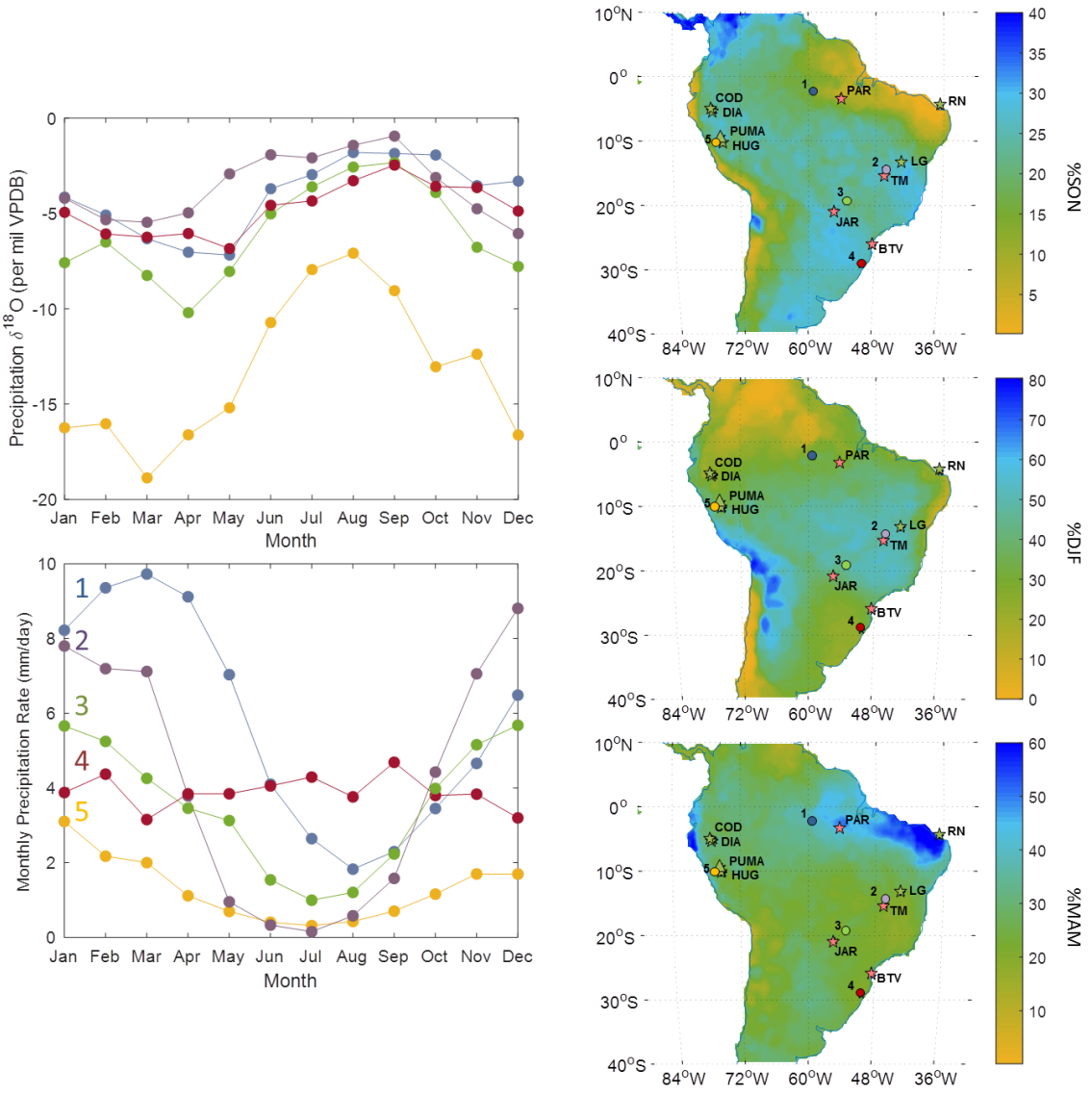

Figure 1: Hydroclimate setting of study region

Maps of $\delta^{18}O$ records from cave (stars) and lake (triangle) sites and Global Network of Isotopes in Precipitation (GNIP) sites with percent of annual precipitation delivered during austral spring (SON, top), summer (DJF, middle), and fall (MAM, (bottom) and monthly mean precipitation amount (bottom) and precipitation $\delta^{18}O$ (top) at GNIP sites (circles). Data from the Global Precipitation Climatology Centre (GPCC) Full Data Reanalysis Version 7 0.5x0.5 Monthly Total Averaged from 1981 to 2010. Pink filled site

markers indicate localities where Sr isotope records were developed for this study. GNIP sites include Manuas (1), Brasilia (2), Campo Grande (3), Porto Alegre (4), and Marcapomacocha (5). Monthly mean precipitation data was calculated using the CPC Merged Analysis of Precipitation (includes NCEP Reanalysis) using the closest grid points to GNIP stations.

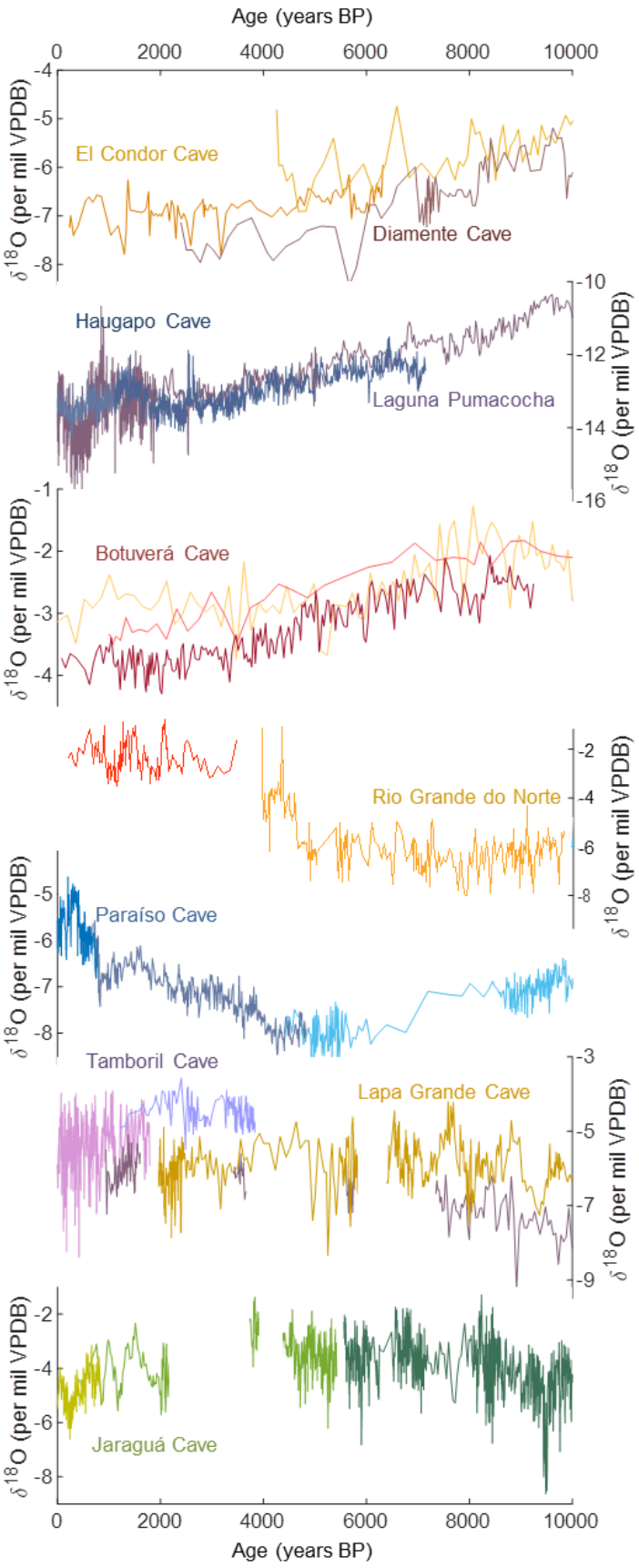
Age (years BP)
0
2000
4000
6000
8000
10000
El Condor Cave
Diamente Cave
Haugapo Cave
Laguna Pumacocha
Botuverá Cave
Rio Grande do Norte
Paraíso Cave
Tamboril Cave
Lapa Grande Cave
Jaraguá Cave
δ18O (per mil VPDB)

Figure 2: Compilation of speleothem and lake core $\delta^{18}O$ records

Different shading in each record indicates a different speleothem from cave site. El Condor Cave (Cheng et al., 2013), Diamante Cave (Cheng et al., 2013), Huagapo Cave (Kanner et al., 2013), Laguna Pumacocha (Bird et al., 2011), Rio Grande do Norte (Cruz et al., 2009), Botuverá Cave (maroon curve - BTV21a, Bernal et al., 2016; yellow curve - BTV2, Cruz et al., 2005; pink curve - BT3, Wang et al., 2007), Paraíso Cave (Wang et al., 2017), Tamboril Cave (pink curve – TM0, Wortham et al., 2017; periwinkle curve – TM2, Wortham et al., 2017; purple curve – TM6, this study), Lapa Grande Cave (Strikis et al., 2011), Jaraguá Cave (dark green curve – JAR07, Novello et al., 2017, mustard green curve – JAR04, Novello et al., 2018, lime green curve – JAR02, Novello et al., 2018b submitted).

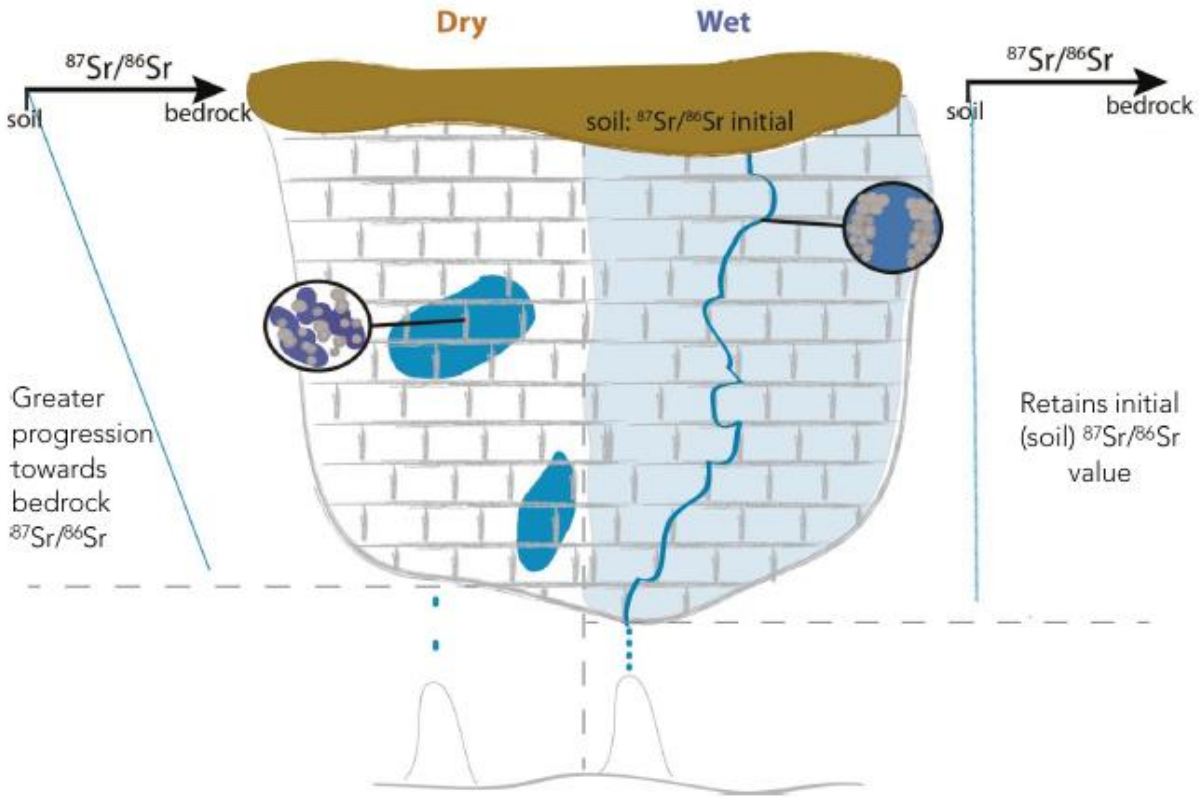

Figure 3: Conceptual model of $^{87}Sr/^{86}Sr$ proxy

$^{87}Sr/^{86}Sr$ variability as a proxy of water rock interaction associated with differences in water residence time under wet and dry conditions. Under dry conditions (left panel), flow through the matrix dominants, enabling greater water rock interaction and greater extent of evolution from the initial $^{87}Sr/^{86}Sr$ composition acquired from the soil toward that of the bedrock. Under wet conditions (right panel), flow through conduit flow paths occurs, limiting water rock interaction and preserving the $^{87}Sr/^{86}Sr$ signature acquired from the soil.

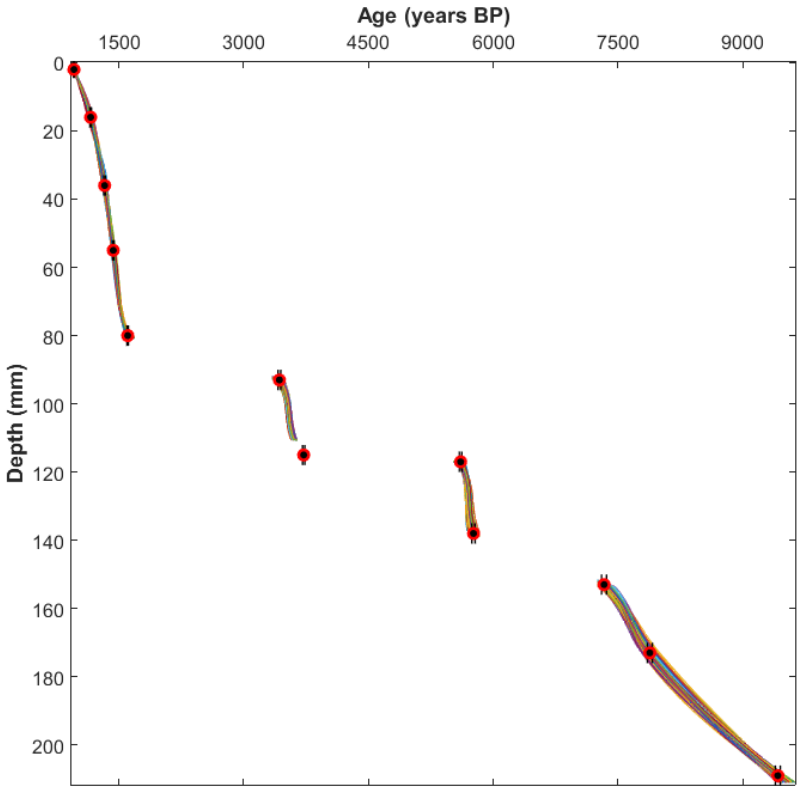

Figure 4: TM6 Age-Model

COPRA developed age-depth model for TM6. The distinct hiatuses are delineated by near-zero slopes and marked as gaps in model.

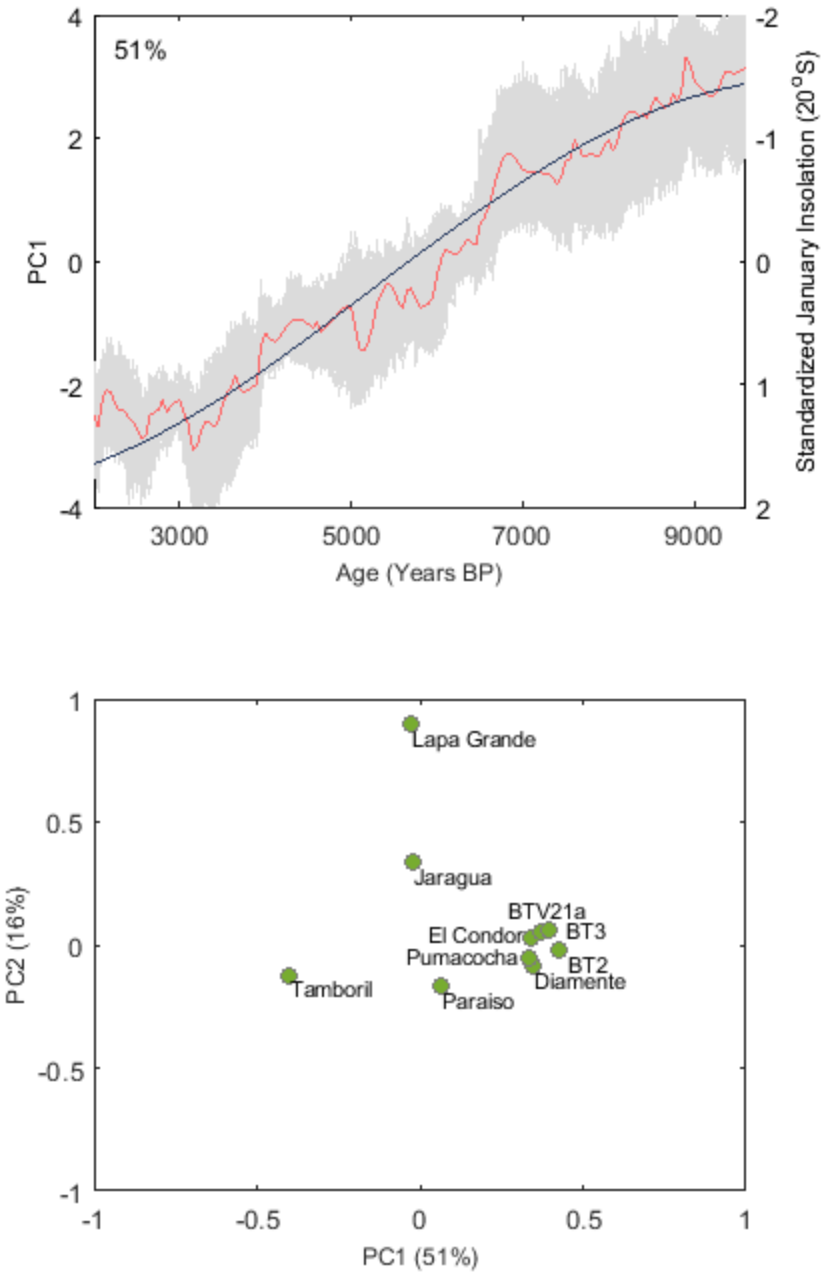

Figure 5: Principle Components Analysis

First principle component from a PCA (pink curve) of compiled $\delta^{18}O$ records from the region, shown relative to austral summer (January) insolation at 20°S (blue curve) (top panel). Weighting of each site on PC1 and PC2 (bottom panel).

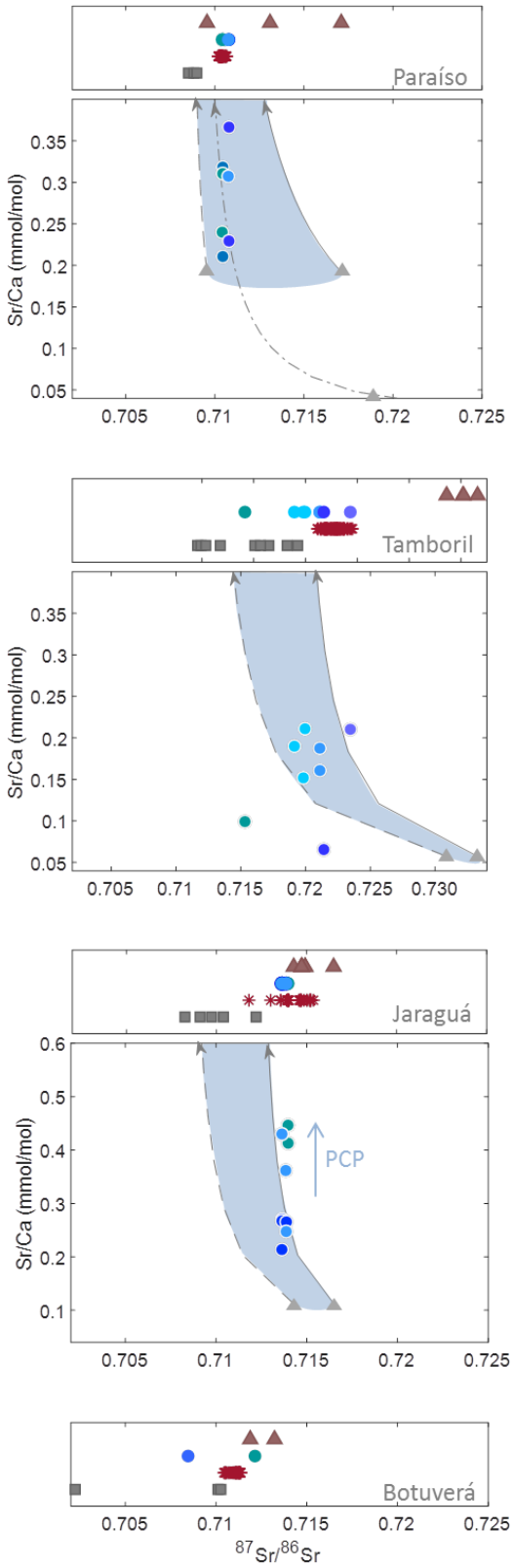
Paraíso
Tamboril
Jaraguá
Botuverá
PCP
Sr/Ca (mmol/mol)
$^{87}Sr/^{86}Sr$

Figure 6: Water-rock interaction modelling

Sr-isotope ($^{87}Sr/^{86}Sr$) values of soil (triangles), bedrock (squares), dripwater (circles), and speleothems (asterisks) from Paraíso, Tamboril, Jaraguá, and Botuverá caves (narrow rectangular panels shown with WRI modelling for Paraíso, Tamboril, and Jaraguá caves (large square panels). Distinct drip sites within each cave are represented by different colors. Grey triangles indicate the starting composition of dripwater. The evolution of dripwater compositions is modelled from the most (solid line) and least (dashed line) radiogenic soil values and lowest Sr/Ca value (i.e., least evolved) measured in dripwater assuming a Sr K_D values of 0.03 based on published experimental range of values (Tesorriero and Pankow, 1996; Terakado and Taniguchi, 2006). Dot-dashed grey line in Paraíso cave represents an idealistic WRI scenario fit to data by changing starting parameters. The blue vertical arrow indicates the evolution of dripwater compositions due to PCP. Shaded area within WRI lines indicates range of possible dripwater values that WRI can account for.

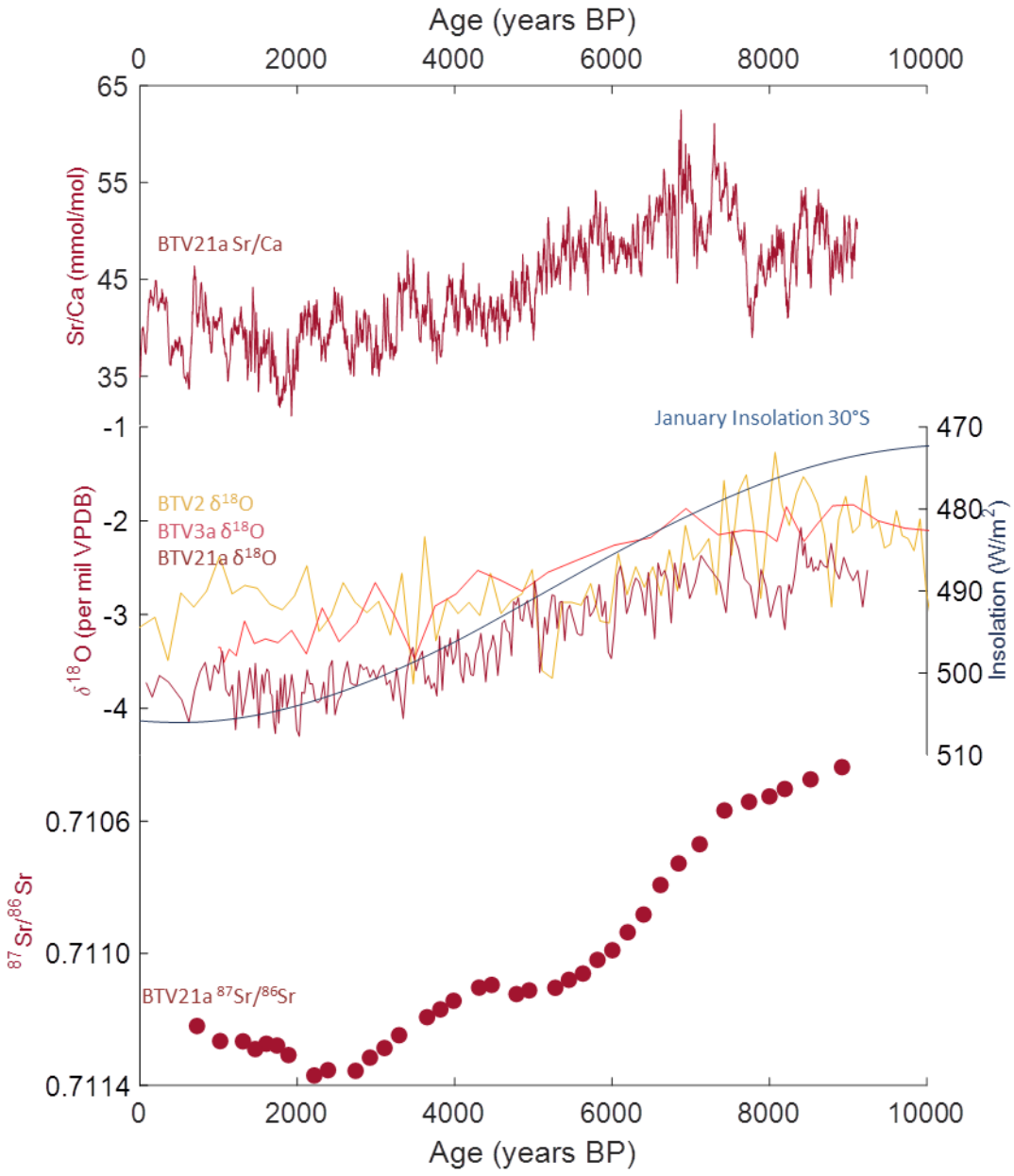

Figure 6: Botuverá Cave proxy records

Comparison of BTV21a Sr/Ca, $\delta^{18}O$, (Bernal et al., 2016) and $^{87}Sr/^{86}Sr$ (this study), and BTV2 (Cruz et al., 2005) and BTV3 (Wang et al., 2007) $\delta^{18}O$ records.

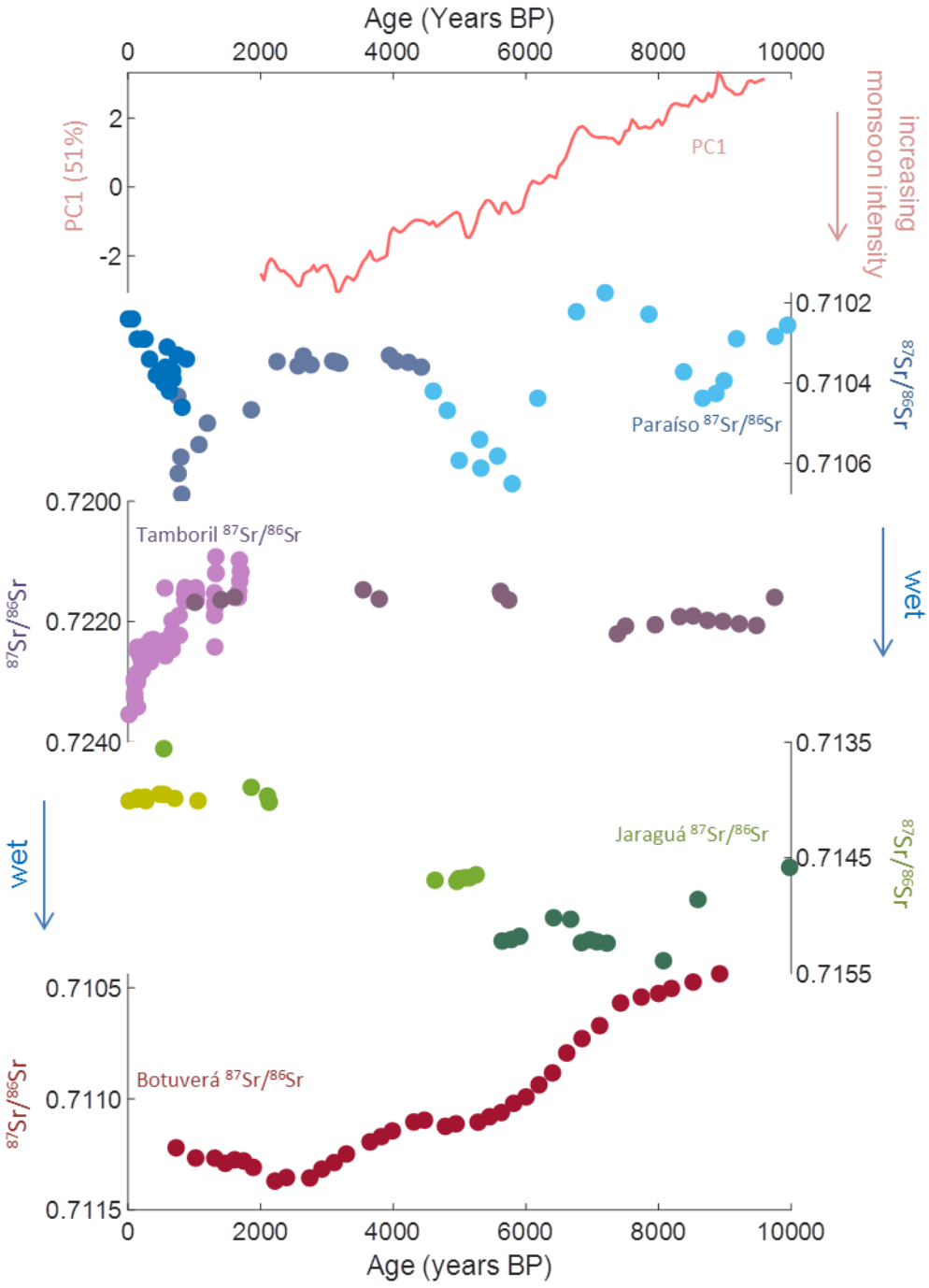

Figure 7: Developed $^{87}Sr/^{86}Sr$ records

Time series of PC1 and Paraíso, Tamboril, Jaraguá, and Botuverá $^{87}Sr/^{86}Sr$ records. $^{87}Sr/^{86}Sr$ axes are flipped so that "wet" conditions interpretation is down.

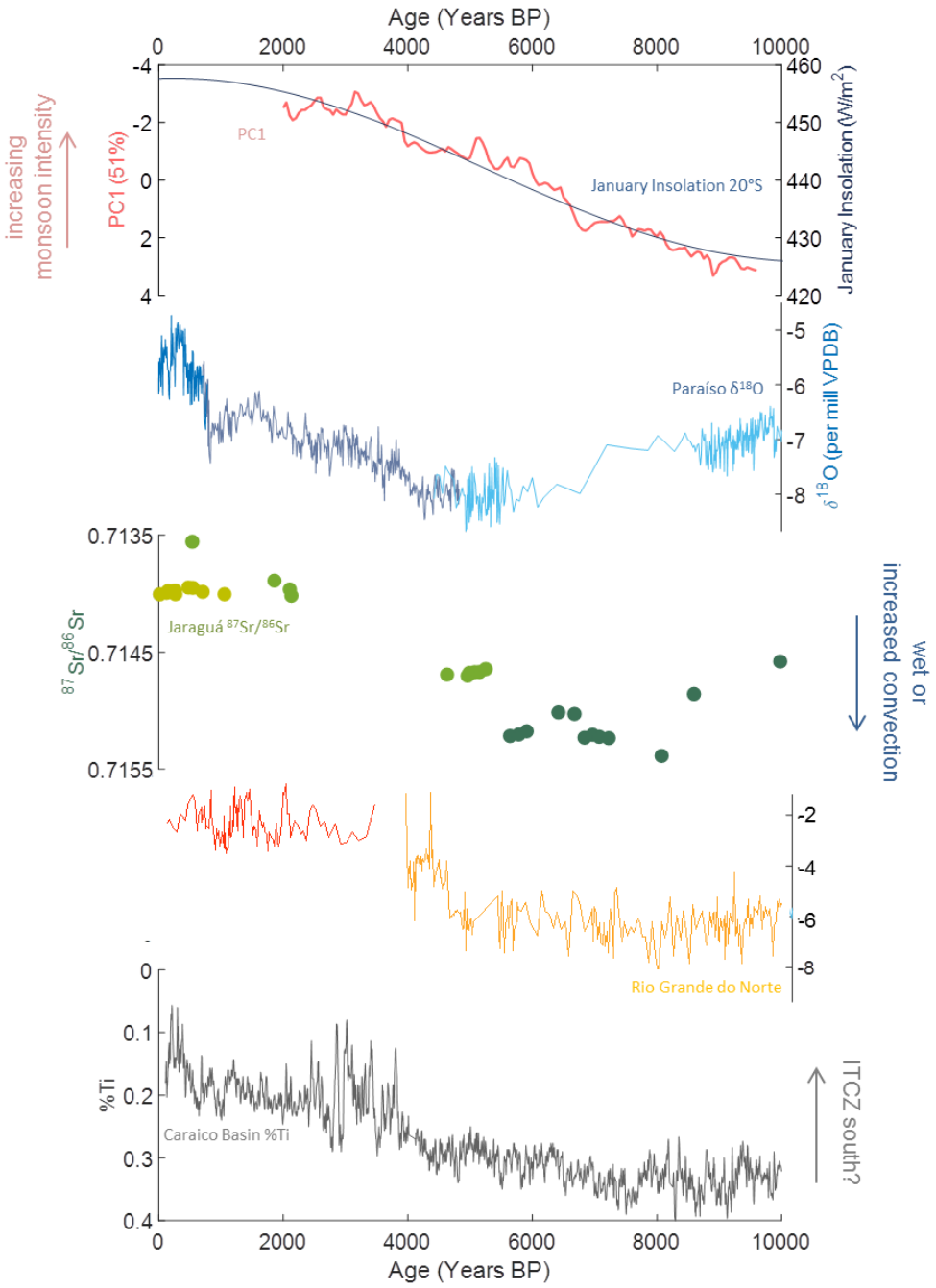

Figure 8: Comparison of similar records

Comparison of PC1, January Insolation at 20°S, Jaraguá $^{87}Sr/^{86}Sr$, Paraíso and Rio Grande do Norte $\delta^{18}O$, and Cariaco Basin %Ti. Axes are flipped for PC1, insolation, $^{87}Sr/^{86}Sr$, and Caricao Basin to readily compare similar trends.

Supplemental Figures

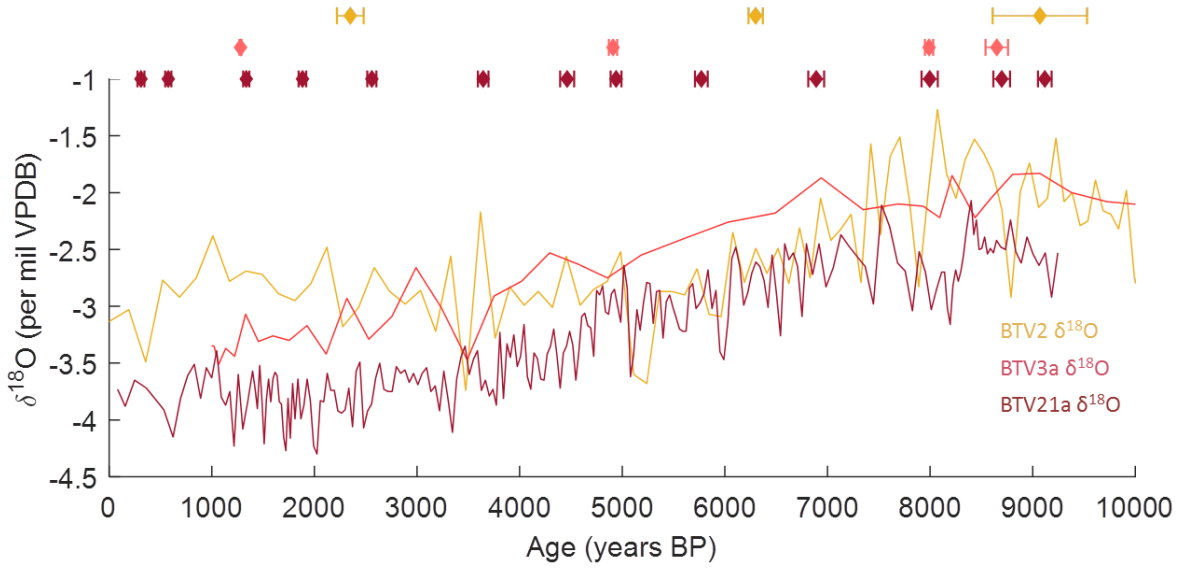

S1: Botuverá $\delta^{18}O$ records

Comparison of BTV2 (yellow), BTV3a (pink), and BTV21a (maroon) speleothem $\delta^{18}O$ records. Diamonds of respective colors indicate U/Th ages and associated error.

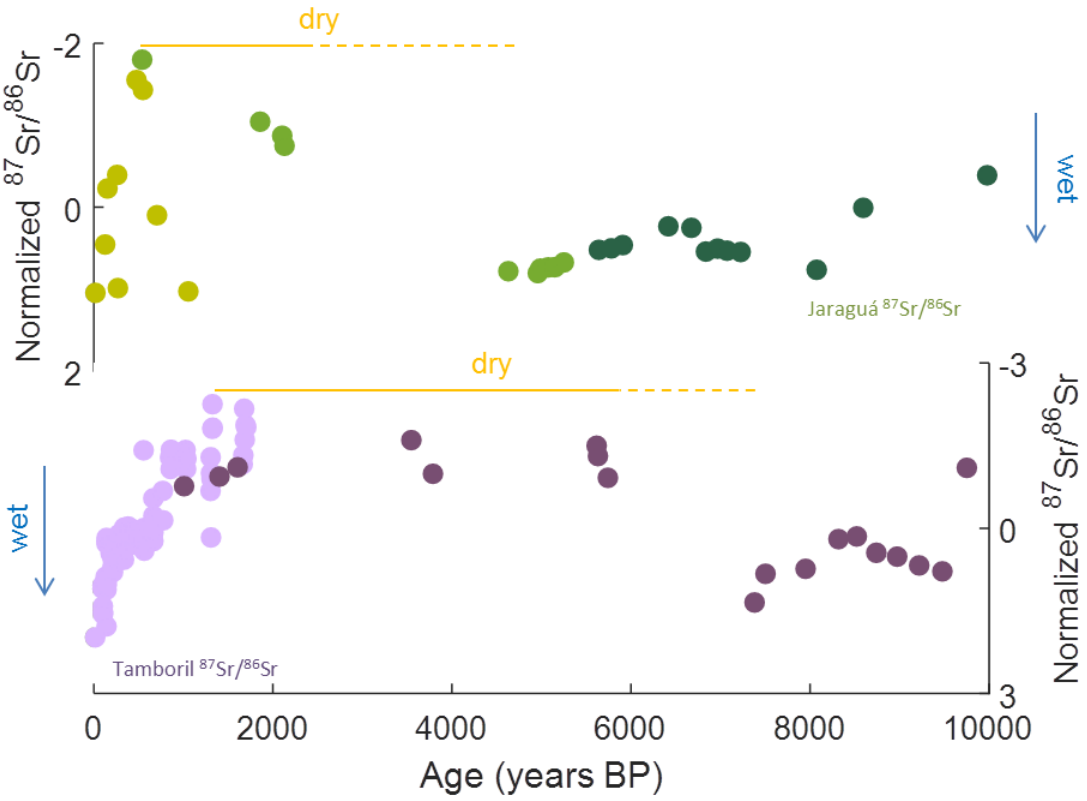

S2: Standardized Tamboril and Jaraguá $^{87}Sr/^{86}Sr$ records

Axes flipped to denote "wet" down interpretation. Yellow arrows indicate step towards dry conditions in individual speleothem samples during mid-Holocene; dashed portion of line indicates a growth hiatus where precise onset of drying conditions cannot be assigned.